PAPER

Check for updates

Assembly of miscible supramolecular network blends using DDA·AAD hydrogen-bonding interactions of pendent side-chains†

Heather M. Coubrough,[a] Matthew Reynolds,[b] James A. Goodchild, [ID] [b] Simon D. A. Connell,[b] Johan Mattsson[b] and Andrew J. Wilson [ID] ⋆[a,c]

The formation of polymer blends can result in materials with superior properties through combination of homo- or co-polymers with divergent functionalities. However, the contrasting physical properties of different polymers often result in phase separation. Herein we induce miscible blend formation of immiscible poly(methyl methacrylate) and polystyrene polymers through triple donor–donor–acceptor and acceptor–acceptor–donor (DDA·AAD) hydrogen bonding between complementary heterodimers on pendent side-chains. RAFT polymerization is used to synthesize a series of poly (methylmethacrylate) and polystyrene co-polymers bearing complementary side-chain hydrogen bonding motifs. Mixing of these polymers promoted miscible blend formation as demonstrated by atomic force microscopy and differential scanning calorimetry. The effectiveness of blend formation was shown to depend upon the extent of incorporation of hydrogen-bonding motif bearing co-monomer; lower degrees of incorporation lead to ineffective blending, whereas higher degree of incorporation, suppress phase separation and promote miscibility.

Introduction

Polymer blends are physical mixtures of two or more polymers that can be either homopolymers or copolymers.[1–4] A major incentive to develop blends is to tune the properties of the individual polymer components, leading to, for instance, enhanced: impact strength, mechanical properties, processability and resistance or stability towards a range of conditions *e.g.* solvent moisture or temperature.[1–5] Modulating properties in this manner has industrial utility *e.g.* in consumer plastics or resins, and in automotive and aircraft industries,[1,3,4,6] where for instance, friction and wear applications require better performance. Polymer blends also offer economic and environmental advantages in terms of the recycling of polymer waste and in developing biodegradable polymers *e.g.* to counter the low viscosity, poor toughness and challenges in re-cycling poly(lactic acid).[7–10] For blending to be viable, the poly-

mers must be compatible, and form stable mixtures. If the polymers are not compatible, phase-separation occurs and where this is significant or changes with time, the system can exhibit undesirable or ill-defined mechanical properties.[11] In general, the behaviour of polymer blends depends on the degree of mixing of the components and their mutual interaction, as well as the individual properties of the components. Blends can be classed as miscible, immiscible or partly miscible. A difference in properties renders many pairs of polymers immiscible on a molecular level (*e.g.* (poly)methyl methacrylate (PMMA) and (poly)styrene (PS)). Indeed, in the majority of cases, the mixing of two polymers results in phase separation.[5,12] Although, the entropy of mixing is always positive for polymer blends leading to a negative contribution to the mixing free energy, the contribution is negligible for long-chain polymers and hence favourable enthalpic interactions are required to promote miscibility.[13] Most combinations of polymers lead to enthalpic contributions to the mixing free energy which are positive and dominate the negative entropic contributions, resulting in phase separation. This is expected given that the properties of individual polymers are influenced by the non-covalent chemistry between polymer chains and differ from backbone to backbone, rendering the design of miscible blends challenging. A generic solution to this challenge would comprise a diverse tool-kit of complementary recognition motifs which can be introduced into immiscible

*[a]School of Chemistry, University of Leeds, Woodhouse Lane, Leeds LS2 9JT, UK.
E-mail: a.j.wilson@leeds.ac.uk*
[b]School of Physics & Astronomy, University of Leeds, Woodhouse Lane, Leeds LS2 9JT, UK
[c]Astbury Centre for Structural Molecular Biology, University of Leeds, Woodhouse Lane, Leeds LS2 9JT, UK
†Electronic supplementary information (ESI) available. See DOI: 10.1039/c9py01913h
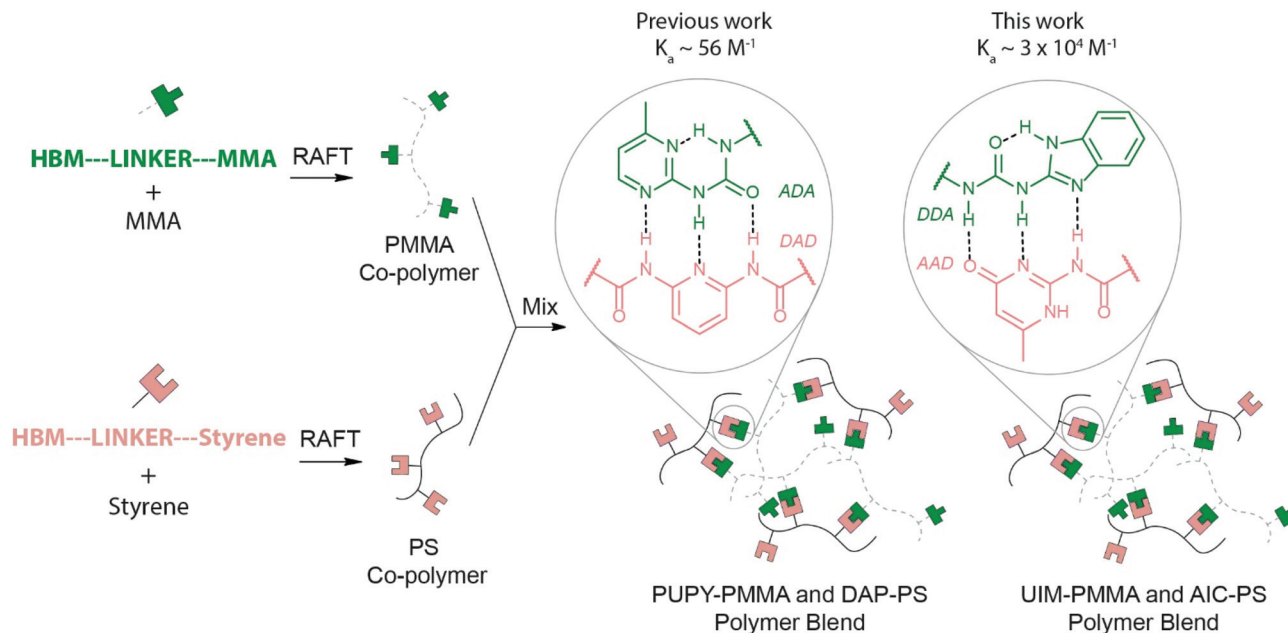
Fig. 1 Schematic outlining the strategy for the formation of a supramolecular blend between PUPY-PMMA (ADA, green) and DAP-PS (DAD, pink) in previous work or UIM-PMMA (ADD, green) and AIC-PS (DAA, pink) co-polymers in this work.

polymer backbones to facilitate tuneable mixing. In this work, we exemplify this alternative and powerful route to achieve blending between otherwise immiscible polymer components. We achieve this by introduction of complementary triple hydrogen bonding motifs into the two immiscible polymers.

Supramolecular polymers have had a profound influence on materials research,[14–16] including the development of self-healing materials,[17] supramolecular adhesives[18] and biomaterials.[19,20] Hydrogen bonding is particularly appealing for supramolecular polymer assembly,[15,21,22] and depends upon the availability of suitable recognition modules *i.e.* hydrogen-bonding motifs (HBMs) motifs.[23–29] To obtain linear supramolecular polymers high affinity HBMs are required,[30] whereas for side-chain-functionalized[31] or cross-linked polymers[32,33] the use of multiple lower affinity HBMs can be used for instance, nucleobases[34,35] and the diamidopyridine/diaminotriazine–thymine dyad (DAP/DAT·T).[36–42] In the context of supramolecular blends, the use of this latter approach exploiting backbones bearing side-chains functionalized with HBMs is desirable. Previously Park *et al.* reported the development of supramolecular polymers using quadruple hydrogen bonding between complementary functionalized macromolecules.[33,43] Supramolecular blends comprising poly(methyl methacrylate) (PMMA) and poly(styrene) (PS) functionalized with acceptor–donor–acceptor (ADA) and donor–acceptor–donor (DAD) HBMs respectively (Fig. 1) were described previously.[44] 14 mol% phenylureidopyrimidine (PUPY; ADA and 6 mol% diamidopyridine (DAP; DAD) was sufficient to promote formation of a miscible polymer blend. However, the ratio of HBM to un-functionalized monomer was high as a consequence of the relatively weak PUPY·DAP affinity ($K_a \sim 56$

M^{-1} in CHCl$_3$).[45] In this work we used a higher affinity ($K_a \sim 3 \times 10^4$ M^{-1})[46] pair of HBMs (Fig. 1): ureidoimidazole (UIM) and amidoisocytosine (AIC)[47,48] with donor–donor–acceptor (DDA) and acceptor–donor–donor (ADD), which, have been used to prepare supramolecular polyurethanes.[49] The use of the UIM·AIC pair allows generation of miscible blends with lower molar ratios of HBM functionalized co-monomers: 2% UIM in PMMA to 5.0% AIC in PS. Such a step allows the use of functionalized co-polymers that are chemically closer to their respective un-functionalized polymers and hence possess more analogous material characterization properties. Moreover the use of orthogonal[50] recognition motifs opens the door to the preparation of self-sorting[51,52] materials[53–55] comprising a greater number of components and opportunities to prepare miscible blends *to order i.e.* where the desired affinity of the HBMs can be selected so as to maximise miscibility for a given pair of polymers.

Results and discussion

The strategy to prepare self-assembled polymer blends with DDA·AAD complementary hydrogen bonding partners is outlined in Fig. 1. UIM-MMA (green) and AIC-styrene (pink) co-monomers **1** and **2** were synthesized (Scheme 1), then co-polymerized using reversible addition fragmentation chain-transfer (RAFT) to form functionalized co-polymers. These co-polymers were subsequently mixed to create a supramolecular polymer blend by evaporation of 1 : 1 mixtures of the polymers in dichloromethane and then characterized by differential scanning calorimetry (DSC) and atomic force microscopy (AFM).
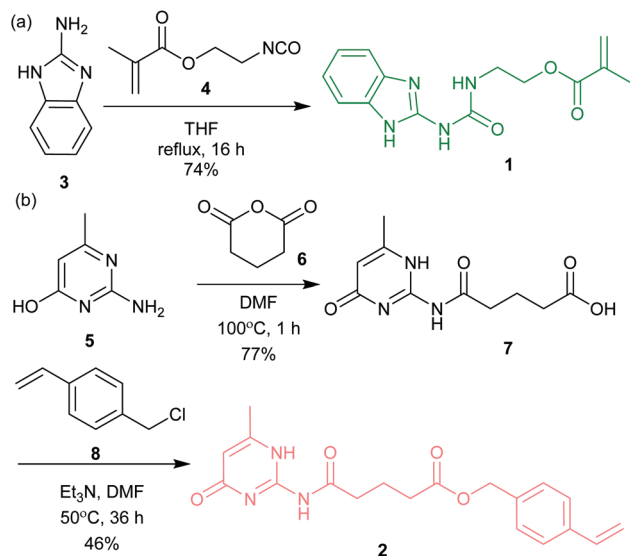
Scheme 1 The synthetic route for preparation of (a) ureidoimidazole methacrylate monomer **1** (UIM–MMA) and (b) amidoisocytosine styrene monomer **2** (AIC–styrene).

Co-monomer synthesis

The polymerizable hydrogen-bonding monomers are comprised of three parts: a hydrogen-bonding moiety and a polymerizable moiety, separated by a linker (Scheme 1). The linker was necessary to limit any electronic influence of proximal functionality on the reactivity of the alkene during RAFT polymerization. This was motivated by previous studies in which direct attachment of the hydrogen-bonding motif to styrene resulted in preferential polymerization over un-functionalized styrene, presumably due stabilization of the reactive radical by the electron-withdrawing hydrogen-bonding motif.[19] Methacrylate functionalized ureidoimidazole monomer (UIM-MMA) **1** was obtained in good yield in one step from 2-aminobenzimidazole **3** and 2-isocyanatoethyl methacrylate **4** (Scheme 1a). The styrene-functionalized amidoisocytosine monomer (AIC-S) **2** was obtained in two synthetic steps (Scheme 1b). The first step was the reaction of 2-amino-4-hydroxy-6-methylpyrimidine **5** with glutaric anhydride **6** to form amide **7** with the hydrogen bonding moiety and linker. The intermediate was then reacted with 4-vinyl-chloride **8** to produce AIC-S **2**. Prior to copolymerization of the functionalized monomers **1** and **2**, with methylmethacrylate or styrene as appropriate, we assessed the impact on the addition of the polymerizable groups on the ability to participate in the expected UIM·AIC triple hydrogen bonding interaction relative to the previously described UIM·AIC complex.[46] Due to low solubility of the UIM-MMA **1** in aprotic solvents, such as $CDCl_3$, ^{1}H NMR analysis was not possible. Consequently, we relied on a molecular modelling study of monomer **1** with **2** carried out using a hybrid Monte Carlo Molecular Mechanics (MCMM) conformational search (see ESI and Fig. ESI 1†). All the conformers retained, with a relative energy within 10 kJ mol^{-1} of the lowest energy conformer (399 in total), displayed the desired DDA·AAD intermolecular hydrogen bonding interaction, as well as the expected intramolecular hydrogen bonds. These analyses indicate that the polymerizable functional groups in UIM-MMA **1** and AIC-S **2** are unlikely to significantly influence dimerization of the UIM·AIC motifs through triple hydrogen bonding.

Polymer synthesis

For creation of polymer blends it was important that incorporation of the hydrogen bonding motifs should not occur in preference to the un-functionalized monomer during polymerization. Whilst a post-polymerization strategy might have proven effective, a "controlled" copolymerization was selected to limit inconsistencies in macromonomer chain lengths and minimize differences in the number and distribution of functionalized monomers within a chain. RAFT polymerization is known as a robust controlled technique which can accommodate a variety of functionalities.[56] Consequently, RAFT was employed for the copolymerization of the functionalized monomers with the corresponding un-functionalized monomers to create a series of PMMA and PS copolymers.

Using a range of UIM-MMA **1**: MMA **9** feed ratios (Table 1), a series of PMMA-based (co)polymers **10–13** were produced following the conditions outlined in Scheme 2a. The commercially available chain transfer agent (CTA) **14** (4-cyano-4-[(dodecylsulfanylthiocarbonyl)sulfanyl]pentanoic acid) was chosen for the synthesis of low molar mass dispersity PMMA-based (co)polymers, together with azobutyronitrile (AIBN) **15** as a radical initiator. A selection of polymer lengths were obtained and in general a small broadening of polydispersity Đ were observed for the copolymers. Polymer **12** was longer, consistent with a longer reaction time. Using ^{1}H NMR analysis, we confirmed that molar incorporation of monomer **1** into the copolymers broadly followed the molar feed ratio, based on the ratio of UIM and MMA integrals. From this, we infer that the hydrogen-bonding motif is randomly distributed within the copolymer backbone rather than clustered in blocks. The synthesized polymers and the corresponding characterization data are collated in Table 1.

Using a range of AIC-S **2**: styrene **16** feed ratios we also prepared a series of PS copolymers **17–21** (Table 1). Cyanomethyl dodecyl trithiocarbonate **22** was the chosen CTA for polystyrene (PS)-based copolymer preparation.[57] Using heat to directly initiate styrene **16** polymerization, we found the conversion was low relative to the PMMA-based copolymers, requiring longer reaction times and resulting in higher Đ (data not shown). We therefore used AIBN **15** as a radical initiator with the aim of increasing the rate of initiation and decreasing the polydispersity of the PS-based copolymers. A pronounced decrease in degree of polymerization and increase in Đ was observed indicating the AIC hydrogen bonding motif monomer **2** to be capable of facilitating termination. Using ^{1}H NMR analysis, we confirmed that molar incorporation of monomer **2** into the copolymers broadly followed the molar feed ratio, based on the ratio of AIC and PS integrals. The synthesized polymers and characterization data are collated in Table 1. As for the MMA

Table 1 Data on un-functionalized polymer and functionalized co-polymers **9–12** and **17–20**

(Co)polymer	Monomer	HBM	HBM molar feed (%)	mol% HBM incorporation	wt% HBM incorporation	M_n (10^3 g mol^{-1})	M_w (10^3 g mol^{-1})	Đ	HB unit per chain	T_g (°C, DSC)
10	9	N/A	0	0	0	28.0	32.9	1.17	0	114
11	9	1	3	2.5	3.0	15.1	20.3	1.34	3.5	111
12	9	1	3	2.0	1.0	39.0	50.2	1.29	7.5	123
13	9	1	6	5.5	4.9	19.1	25.2	1.31	9.0	113
17	16	N/A	0	0	0	25.6	34.0	1.33	0	98
18	16	2	1	1.5	1.2	16.0	28.3	1.77	2.0	96
19	16	2	3	2.0	2.8	8.1	16.2	2.01	1.5	98
20	16	2	6	5.0	6.8	8.1	16.6	2.04	3.5	98
21	16	2	6	5.5	6.0	11.4	20.8	1.82	5.5	100
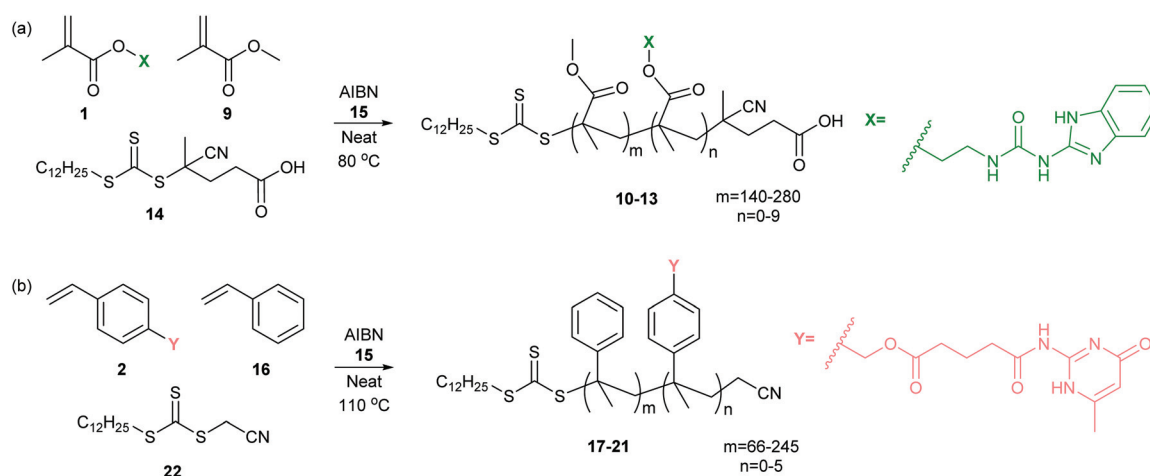
Scheme 2 Synthesis of co-polymers **10–13** and **17–21** using RAFT (a) MMA **9** and MMA-UIM co-monomer **1** and (b) styrene **16** and PS-AIC co-monomer **2**.

copolymers we infer a random distribution of hydrogen bonding monomers within the polymer chain. For clarity: in the following sections, the polymers are named according to the mol% incorporation of HBM.

Blend characterization

Differential scanning calorimetry (DSC) characterisation. Blend formation was characterized using DSC and AFM. For the DSC experiments, blend samples were prepared by dissolving the polymers into dichloromethane followed by solvent casting (see methods for details). In our previous study,[44] samples were not heated above 100 °C to avoid thermal radical re-initiation. In the present study, the experiments were performed with a temperature limit >100 °C; although for some samples, the glass transition temperature T_g was near or above the 100 °C limit, re-initiation is unlikely to have occurred which is supported by the evidence that subsequent heating and cooling cycles (between 20 °C and 180 °C) revealed a consistent T_g.

The heat flow measured on cooling for the two control polymers **10** (PMMA) and **17** (PS) together with a 1:1 blend of the

two polymers is shown in Fig. 2a (see Fig. ESI 2† for all individual polymers). For both PMMA and PS, the glass transitions are clearly observed as exothermic steps upon cooling and the T_g values determined as the inflection points thus characterize the transition midpoints. We obtain a T_g value of 98 °C for PS and 114 °C for PMMA, respectively, which are consistent with previously reported literature values;[58] the T_g-values are marked with vertical dashed lines. The 1:1 blend of the two polymers (**10** and **17**) shows two distinct T_g's characterised by steps at 114 and 98 °C, respectively.

To further clarify the transition behaviour, the temperature derivative of the data in Fig. 2a are shown in Fig. 2b, where it is clear that the blend data correspond to two separate glass-transitions. Moreover, the transitions of the pure polymer components are unchanged by the formation of the blend (Fig. 2a and b), supporting the immiscibility of PMMA and PS, which is well known[59] (data for the corresponding heating runs are shown in the Fig. ESI 3†).

The temperature dependent heat flow of the co-polymer **12** (2% PMMA-UIM) and the functionalized co-polymer **20** (5.0% PS-AIC) together with a 1:1 blend of the two components are
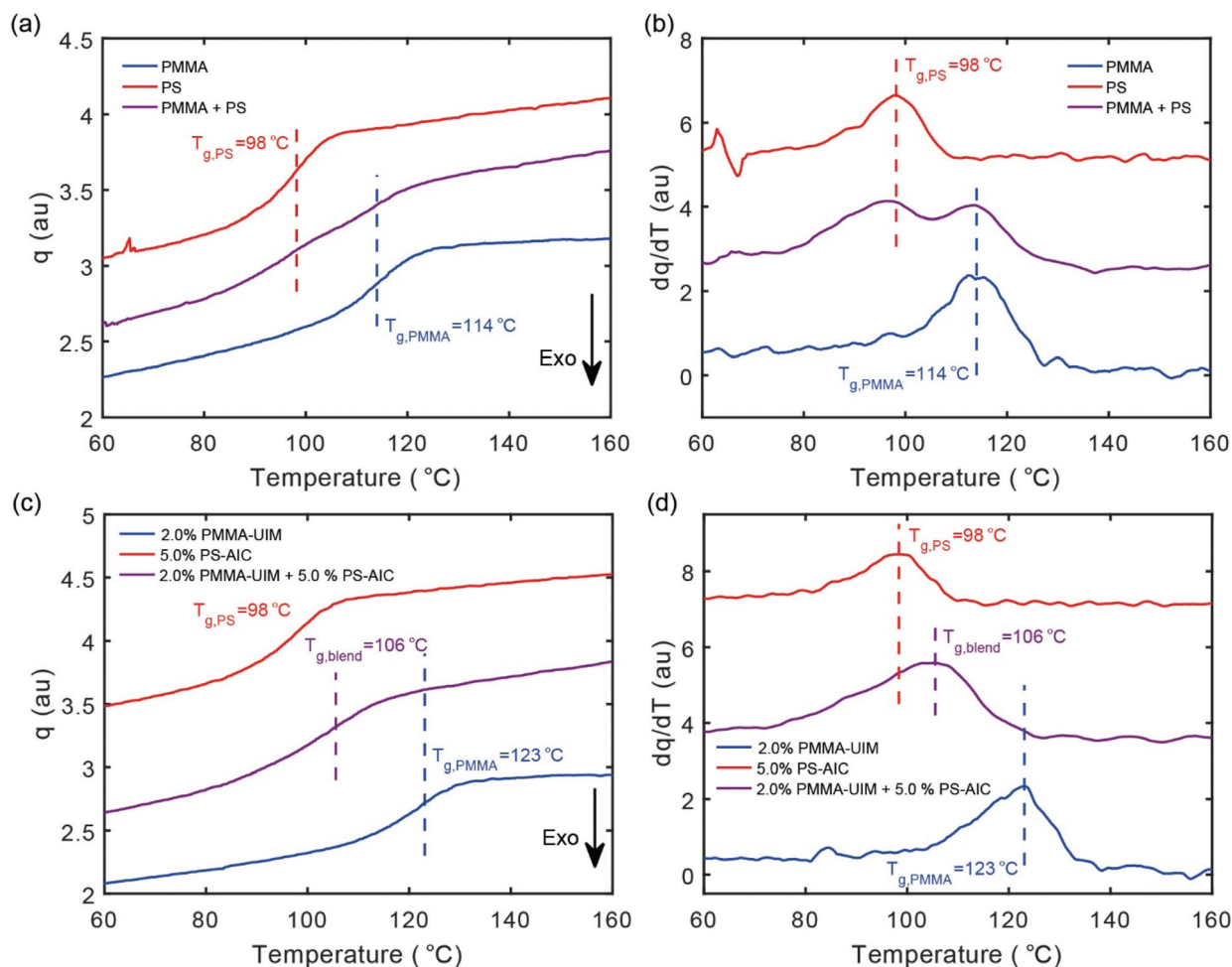
Fig. 2 DSC thermogram of temperature against (a, c) heat flow and (b, d) first derivative of heat flow on cooling of (a, b) control sample: polymer **10** (PMMA) with polymer **17** (PS) and (c, d) blended sample: PMMA co-polymer **12** (2% PMMA–UIM). PS co-polymer (5.0% PS-AIC) **20** in red, PMMA in blue and blend in purple.

shown in Fig. 2c; the corresponding temperature derivatives are shown in Fig. 2d. The T_g-value of co-polymer **20** (5.0% PS-AIC) is 98 °C and thus very similar to that of the un-functionalized PS **17**, demonstrating that the modification of PS does not significantly change its T_g-value. In contrast, the T_g-value for co-polymer **12** (2.0% PMMA–UIM) is 123 °C, compared with the 114 °C of the un-functionalized PMMA **10**; thus the functionalization increases the T_g-value by 8 °C. We have shown using DSC (Fig. ESI 2†) that the degree of copolymerization with functionalized groups does not greatly alter the calorimetric response either for PMMA or PS; however, polymer **12** (2% PMMA–UIM) does show a T_g increase of 8 °C compared to the other co-polymers. It is not fully clear why this is, but the observation might be reconciled by that the fact that the co-polymer **12** (2% PMMA–UIM) has a higher degree of polymerization in comparison to un-functionalized PMMA **10** (Table 1).

Significantly, the 1 : 1 blend of the two polymer components shows a broad glass-transition signature with a peak temperature of T_g = 106 °C, situated between the T_g's of the two blend

components, a result which is consistent with a significant increase in compatibility and thus blend miscibility. In a previous study on blends exploiting a ADA·DAD hydrogen-bonding interaction,[44] 14 mol% (16 wt%) of the ADA and 6 mol% (5 wt%) of the DAD hydrogen bonding motifs were required for blending of the respective PMMA and PS co-polymers. Here, a similar effect was achieved using a AAD·DDA interaction with only 2.0 mol% (1 wt%) and 5 mol% (7 mol wt%) of the UIM and AIC motifs respectively. Hence the stronger dimerization affinity translates to supramolecular polymer blends and consequently could result in the creation of supramolecular polymers with lower percentages of hydrogen bonding motifs with material properties close to those of un-functionalized polymers. However, the fact that the amount of HMB required in the polystyrene compound is comparable between the two studies emphasises that (inter-polymer) hydrogen-bond affinity is not the sole determinant for effective miscibility (see further discussion below). We also note, that the low-T flank of the broad transition coincides quite well with the transition of the pure 5.0% PS-AIC component, as

shown most clearly in the derivative data representation of Fig. 2b on cooling (see Fig. ESI 3† for heating). We note that two separate glass transitions can sometimes be observed even for polymer blends with a good compatibility.[60] This could be explained by the fact that a polymer chain will over some length-scale be primarily surrounded by itself, leading to an effective "self-concentration". For some polymer combinations this can thus lead to a blend with two separate glass transitions and two corresponding T_g values even for a compatible polymer combination.[60] These effects have been observed *e.g.* for blends of polyethylene oxide and PMMA,[61] and for polyiso-prene and poly(4-*tert*-butylstyrene).[62] Thus, whilst functionalization of PMMA and PS with HBMs results in a significant increase in compatibility as demonstrated by calorimetry, quantification of the effectiveness of this approach requires complementary characterisation which we achieve using atomic force microscopy (AFM), as discussed below.

To further explore the limitations on the formation of compatible blends using the AIC·UIM motif we carried out further DSC experiments on blends made from polymers with different HBM incorporation (see ESI† for details). We observed that at lower levels of HBM incorporation, a significant increase of the blend compatibility did not occur. For both co-polymer **11** (1.5% PMMA-UIM) mixed with functionalized co-polymer **18** (1.5% PS-AIC) and co-polymer **11** (1.5% PMMA-UIM) mixed with functionalized co-polymer **19** (2.0% PS-AIC), two distinct transitions were observed in the DSC results on the blended sample (Fig. ESI 4 and 5† respectively). In both cases, the high-T_g component putatively associated with the PMMA-based polymer component increases (by ~10 °C), whereas the low T_g component stays roughly unchanged. More surprisingly, indications of miscible blend formation with higher levels of HBM incorporation were less pronounced using DSC; for co-polymer **13** (5.5% PMMA-UIM) mixed with functionalized co-polymer **21** (5.5% PS-AIC), two T_g's were observed, with the second again showing an increase relative to co-polymer **13** (5.5% PMMA-UIM) on its own (Fig. ESI 6†).

The ability to blend at the molecular level through hydrogen bonding is influenced by a number of factors: (i) the strength of hydrogen bonds; (ii) the number of HBMs on each chain; (iii) the ability of the HBMs to (self-)stack (and or their crystallinity). The observations collectively can be explained as follows: as expected at lower levels of HBM incorporation there are insufficient numbers of HBMs on each polymer to promote good mixing, whilst at higher levels of HBM incorporation there maybe too many and these could self-stack through π–π interactions or self-associate through intra-polymer hydrogen-bonding, to compete with inter-polymer hydrogen-bonding and heterodimerization. ^{1}H NMR analyses on blended samples indicate a change in hydrogen-bonding on mixing, however infrared analyses were unable to provide further experimental insight and a more detailed study will be pursued in due course (see ESI Fig. ESI 7 and 8†). The apparent increase in T_g in the PMMA-related transitions may arise as a consequence of forming a partially

miscible blend whereby there is some hydrogen-bonding between PS and PMMA domains, but also stacking and aggregation. In addition, as noted above, two separate glass transitions can be observed also in some miscible blends. Hence we explored this further using AFM analyses on mixtures of polymers, as discussed in the next section. Finally, the increased degree of polymerization of the co-polymer **12** (2% PMMA-UIM) points to a role for degree of polymerization in controlling blending at higher molecular weights where the number of non-covalent "contact points" between chains could be greater.

AFM characterisation. To explore the phase behaviour at the nanoscale, AFM experiments were performed on blended samples (see methods). The polymers were dissolved in dichloromethane and spin cast onto a silicon wafer surface upon which they were dried under vacuum for 24 hours at 120 °C before the measurements. The AFM images for the control samples of PMMA **10** and PS **17** clearly demonstrate phase separation as observed in the height profile image in Fig. 3a, and at a higher magnification in Fig. 3b. Line profiles beneath each image panel show phase segregated structures with a typical height of 10 nm, whilst image analysis gives a domain size of 540 nm (s.d. = 110 nm, N = 164). The area fraction of each phase is 50 ± 5%. The two observed phases (PMMA and PS) are also clearly shown in Fig. 3c in a PF-QNM AFM elastic DMT modulus map, displayed on a logarithmic scale. Histograms of the modulus map show a clear separation of moduli where one domain phase is characterized by a mean modulus of 3.9 GPa and the other matrix phase by 3.0 GPa. The PF-QNM mode had been pre-calibrated on a PS/LDPE standard to give a PS modulus of 3.0 GPa, thus indicating that the matrix phase is PS. However, moduli of polymer thin films as measured by various nanoindentation techniques can vary depending upon temperature, load, film thickness and contact model used.[63–65] The thickness of the PMMA/PS film was 125 nm, comfortably above the critical film thickness of approximately 50 nm, below which the measured modulus would substantially increase.[65] All other parameters are identical, so comparison of moduli values between samples is valid. Typical literature values found by nanoindentation on similarly prepared samples are for PMMA = 3.3 ± 0.5 GPa/PS = 2.6 ± 0.2 GPa,[65] PMMA = 4.1 GPa/PS = 3.0 GPa,[64] and PMMA = 5.5 GPa/PS = 4.3 GPa, showing that PMMA has a modulus that is reproducibly 30% higher than PS.[63] This is identical to the difference shown here, thus we confidently assign the 'lighter' 3.9 GPa domains in Fig. 3c to PMMA, and the darker 3.0 GPa matrix to PS. This structure is typical of immiscible polymer blends, as previously demonstrated.[59] To further demonstrate the utility of the modulus mapping, Fig. ESI 9† shows a high force (approximately 100 nN) nanoindentation scratch across one of the observed domains, as shown in the (a) height, (b) peak force error signal and (c) modulus map. The PF-QNM modulus contrast correlated perfectly with penetration of the sharp AFM tip, with a heavy 5.2 nm deep scratch observed on the lower modulus (softer) polystyrene matrix, and a light 0.3 nm deep scratch on the higher modulus (stiffer) PMMA
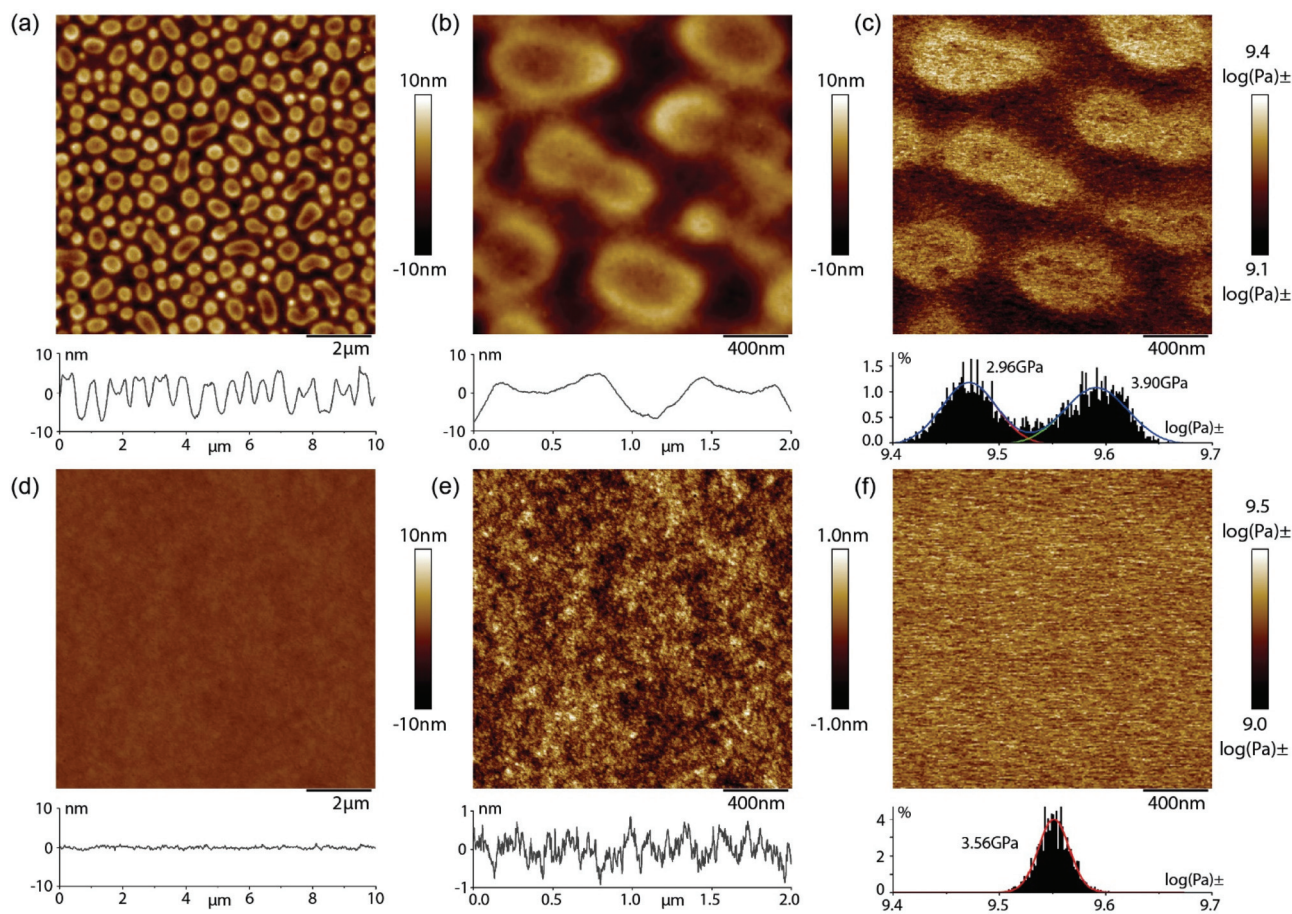
Fig. 3 AFM analyses of blended comprising 1:1 mixture of un-functionalized PMMA **10** and PS **17** (a–c) or AIC-PMMA **12** and AIC-PS **20** (d–f) showing height images at 2 mM an (a, d) and 400 nM (b and e) together with rheological analysis (c and f).

domain. Nanometre scale nanoindentation scratches and pits on polymers will recover over time, so the absolute values of these scratch depths cannot be used as a facile method to judge modulus.

In contrast, the AFM images of the blend comprising the co-polymer **12** (2% PMMA-UIM) and co-polymer **20** (5.0% PS-AIC) demonstrates a very high degree of miscibility on the nanoscale. The surface of the 103 nm thick film is flat and featureless (Fig. 3d) and magnification of the height scale reveals a fine textured surface with height variations around 1 nm (Fig. 3e). The highly compatible nature of the blend is further illustrated by the modulus measurement which demonstrates a single phase and a mean modulus of 3.6 GPa, which is situated between the moduli of pure PMMA and PS, as observed in Fig. 3c. High magnification views of the blend sample are shown in Fig. ESI 10a† along with simultaneously acquired nanomechanical channels of elastic DMT modulus (Fig. ESI 10b†), surface deformation (Fig. ESI 10c†), and adhesion (Fig. ESI 10d†). The contrast in the modulus image is very weak, but shows regions of contrast variation on a scale <50 nm. These structural fluctuations are more clearly observed in the surface deformation and adhesion channels. Thus, very weak and small length-scale fluctuations are

observed on small scales, but no indication of any significant phase segregation is observed in support of the DSC results demonstrating a significantly increased blend compatibility. We also obtained AFM data on the blend comprising the co-polymer **13** (5.5% PMMA-UIM) mixed with functionalized co-polymer **21** (5.5% PS-AIC), (see Fig. ESI 11†); these also indicate good miscibility on the nanoscale (see ESI†). Interestingly, however, the mean modulus of 4.9 GPa is higher than either pure PMMA or PS and point to more complex behaviour as is suggested by the DSC data.

Conclusions

We have designed analogues of styrene and methyl methacrylate polymerizable monomers functionalized with the HBMs ureidoimidazole (UIM) and amidoisocytosine (AIC) bearing donor–donor–acceptor (DDA) and acceptor–acceptor–donor (ADD) arrays respectively. RAFT polymerization was used to prepare a series of PMMA and PS co-polymers with varying degrees of complementary functionalized HBMs. AFM and DSC analyses of the resultant supramolecular assemblies demonstrate the power of the approach for making miscible

blends. Miscible polymer blends were obtained for mixtures of functionalized co-polymers of PMMA and PS, while PMMA and PS in the absence of hydrogen bonding arrays were shown to be immiscible, thus emphasizing the requirement of hydrogen bonding motifs to induce blend formation. This work, taken together with previously reported HBM functionalized side-chain supramolecular polymers,[44] highlights the ability of hydrogen bonding to overcome the inherent phase separation behaviour of immiscible polymers. More broadly these preliminary studies exemplify the power of an expanded supramolecular toolkit with which miscible blends can be prepared *to order*, with HBMs selected based on the strength of dimerization and knowledge of the immiscibility of the component polymers, to ensure maximum similarity and therefore properties to the respective un-functionalized polymers. Such studies together with the development of multi-component blends that exploit self-sorting[51,52] will represent the focus of our future studies.

Experimental

General considerations for synthesis

Solvents and reagents were purchased from Sigma Aldrich, Fisher Scientific or fluorochem and used without further purification unless otherwise stated. Where anhydrous solvents were required, dichloromethane, chloroform, tetrahydrofuran and acetonitrile were obtained from the in-house solvent purification system Innovative Inc. PureSolv®. Anhydrous dimethyl formamide and *N*,*N*-diisopropylethylamine were obtained from Sigma Aldrich equipped with Sure/Seal™. All non-aqueous reactions were carried out under a nitrogen atmosphere. For reactions under non-anhydrous conditions, the solvents used were HPLC quality and provided by Fisher or WVR. Water in aqueous solutions and used for quenching was deionised. Mixtures of solvents are quoted as ratios and correspond to a volume : volume ratio. Analytical thin layer chromatography was performed on Merck Kieselgel 60 F254 0.25 mm pre-coated aluminium plates. Product spots were visualised under UV light (λ_{max} = 254 nm) or using a suitable stain. Flash chromatography was carried out using Merck Kieselgel 60 silica gel using pressure by means of head bellows or using disposable RediSepRf silica flash columns on an automated Biotage Isolera One system. Nuclear magnetic resonance spectra were obtained at 298 K (unless stated) using a Bruker AV500 spectrometer operating at 11.4 T (500 MHz for ^{1}H and 125 MHz ^{13}C) as stated. Infra-red spectra were obtained using a Bruker Alpha Platinum ATR where absorption maxima (ν_{max}) are quoted in wavenumbers (cm^{-1}) and only structurally relevant absorptions have been included. High Resolution Mass Spectra (HRMS) were recorded on a BrukerDaltonicsmicroTOF using electrospray ionisation (ESI). Liquid Chromatography and Mass Spectrometry (LC-MS) was performed using an Agilent Technologies 1200 series LC and a Bruker HCT ultra ion-trap MS. Gel permeation chromatography (GPC) measurements were conducted using Waters Acquity APC system fitted

with three 2.4 μm columns plus a guard column and a refractive index detector. DMF and THF eluent was used at a flow rate of 0.5 mL min^{-1} and temperature of 40 °C. A series of 6 near-monodisperse poly(methylmethyacrylate) standards in DMF and near-monodisperse polystyrene standards in THF (M_w ranging from 2000 to 100 000 g mol^{-1}) were employed as calibration standards in conjunction with RI detector for determining molecular weights.

Monomer synthesis

2-(3-1*H*-Benzo[*d*]imidazol-2-ylureido)ethyl methacrylate 1. A solution of 2-aminobenzimidazole **3** (786 mg, 5.90 mmol) in anhydrous tetrahydrofuran (12 mL) was stirred at reflux under nitrogen atmosphere for 3 h. 2-Isocyanatoethyl methacrylate **4** (1.00 mL, 7.08 mmol) was then added dropwise to the reaction mixture over 10 minutes. The reaction was stirred at reflux for a further 20 h. The precipitate was isolated and dried under vacuum to give 2-(3-1*H*-benzo[*d*]imidazol-2-ylureido)ethyl methacrylate as a colorless solid; (1.26 g, 4.37 mmol, 74%) ^{1}H NMR (500 MHz, DMSO-d_6) δ 11.45 (br. s., 1H, N*H*), 9.99 (br. s., 1H, N*H*), 7.73 (br. s., 1H, N*H*), 7.25–7.45 (m, 2H, Ar–*H*), 7.03 (dd, J_1 5.58, J_2 3.06, 2H, Ar–*H*), 6.15–6.06 (m, 1H, CC*H*H′), 5.75–5.69 (m, 1H, CC*H*H′), 4.23–4.17 (m, 2H, OC*H*$_2$), 3.56–3.48 (m, 2H, NHC*H*$_2$), 1.98–1.86 (m, 3H, C*H*$_3$) ppm; ^{13}C NMR (125 MHz, DMSO-d_6) δ 166.5, 154.4, 148.4, 135.9, 125.6, 120.5, 120.5, 113.5, 63.5, 38.4, 17.8 ppm; ν_{max} (solid state) = 3341, 2941, 1707, 1531 cm^{-1}; ESI-HRMS *m/z* found 311.1114 [M + Na]$^+$ C$_{14}$H$_{16}$N$_4$NaO$_3$ requires 311.1115.

4-[(6-Methyl-4-oxo-1,4-dihydropyrimidin-2-yl)carbamoyl]butanoic acid 7. Glutaric anhydride **6** (10.9 g, 96.0 mmol) and 2-amino-4-methyl-6-hydroxypyrimidine **5** (10.0 g, 80.0 mmol) were heated at 100 °C in anhydrous dimethylformamide (150 mL) for 2 hours. The mixture was cooled to room temperature and the product was triturated on addition of methanol. The precipitated was filtered and dried to give 4-[(6-methyl-4-oxo-1,4-dihydropyrimidin-2-yl)carbamoyl]butanoic acid as an off-white solid (13.7 g, 57.5 mmol, 72%); ^{1}H NMR (400 MHz, DMSO-d_6): δ 11.79 (br s, 2H, N*H*), 5.92 (s, 1H, imidazole-*H*), 2.46 (t, *J* 7.3, 2H, OCOC*H*$_2$), 2.27 (t, *J* 7.3, 2 H, NHCOC*H*$_2$), 1.82–1.74 (m, 2H, CH$_2$C*H*$_2$CH$_2$) ppm; ^{13}C NMR (100 MHz, DMSO) δ 176.5, 174.4, 165.2, 161.1, 150.8, 107.4, 35.6, 33.1, 23.7, 20.0 ppm; ν_{max} (solid state) = 3207, 2917, 1663, 1577 cm^{-1}; ESI-HRMS *m/z* found 240.0976 [M + H]$^+$ C$_{10}$H$_{14}$N$_3$O$_4$ requires 240.0979.

(4-Ethenylphenyl)methyl 4-[(6-methyl-4-oxo-1,4-dihydropyrimidin-2-yl) carbamoyl]butanoate 2. A suspension of 4-[(6-methyl-4-oxo-1,4-dihydropyrimidin-2-yl)carbamoyl] butanoic acid **7** (2.00 g, 8.36 mmol) and anhydrous triethylamine (0.97 mL, 6.97 mmol) in anhydrous dimethylformamide (100 mL) was heated to 100 °C until a solution was reached. The reaction was cooled to 50 °C and 4-vinylbenzyl chloride **8** (0.98 mL, 6.97 mmol) was added dropwise over 1 hour. The reaction was stirred at 50 °C for 48 hours. The reaction mixture was cooled and poured onto water. The resulting precipitate was filtered and filtrate was extracted with ethylacetate (5 × 50 mL). The organic layer was reduced in volume, combined

with the precipitate and washed with brine (5 × 50 mL), dried over sodium sulfate, filtered and concentrated under reduced pressure. The product was purified by column chromatography (SiO$_2$, 5 : 95 methanol : dichloromethane) to yield (4-ethenyl-phenyl)methyl 4-[(6-methyl-4-oxo-1,4-dihydropyrimidin-2-yl) carbamoyl]butanoate as an off-white solid (1.14 g, 3.20 mmol, 46%); ^{1}H NMR (500 MHz, CDCl$_3$): δ 7.04 (d, J 8.2, 2H, Ar–H), 7.31 (d, J 8.2, 2H, Ar–H), 6.71 (dd, J_1 17.3, J_2 11.2, 1H, CHCHH'), 5.99 (s, 1H, Py–CH), 5.75 (d, J 17.3, 1H, CHCHH′), 5.27 (d, J 11.2, 1H, CHCHH'), 5.11 (s, 2H, Bn–CH_2), 2.60–2.51 (m, 2H, OCOCH_2), 2.49 (t, J 7.2, 2H, NHCOCH_2), 2.12–1.99 (m, J 7.2, 2H, CH$_2$CH_2CH$_2$) ppm; ^{13}C NMR (125 MHz, CDCl$_3$): δ 172.7, 166.1, 162.7, 149.3, 137.6, 135.3, 128.4, 126.4, 114.4, 108.0, 66.2, 35.9, 33.1, 23.9, 19.8 ppm; ν_{max} (solid state) = 3118, 3061, 2945, 2888, 1731, 1664 cm^{-1}; ESI-HRMS m/z found 356.1621 [M + H]$^+$ C$_{19}$H$_{21}$N$_3$O$_4$ requires 356.1566.

General procedure for PMMA-co-UIM-MMA polymerization. The required amount of UIM-MMA **1** (if required) and solvent (if required) was transferred to an ampoule with stirrer bar under nitrogen atmosphere. A solution of the required amount of 4-cyano-4-((dodecylsulfanylthiocarbonyl)sulfanyl) pentanoic acid (CTA) **14** and azobutyronitrile (AIBN) **15** (if required) dissolved in methyl methacrylate monomer **9** was also prepared, and the required aliquot of stock solution was added to the ampoule by syringe addition. The reaction mixture was thoroughly degassed by purging with nitrogen for 30 minutes, followed by three freeze–pump–thaw cycles. The reaction mixture was placed into a preheated oil bath at 80 °C and stirred for the specified time. After this time, the flask was immediately cooled to 0 °C to prevent any further polymerization. Precipitation with methanol twice, followed by removal of residual solvent under reduced pressure provided the title material as a flocculent colorless powder.

PMMA 10. General procedure for PMMA-co-UIM-MMA polymerization was followed adding methyl methacrylate (1.60 mL, 15.0 mmol), 4-cyano-4-((dodecylsulfanylthiocarbonyl)sulfanyl) pentanoic acid **14** (12 mg, 0.03 mmol) and AIBN **15** (1 mg, 0.006 mmol) to a schlenk tube and heated for 18 hours. Yield: 1.35 g, 89%; M_n (g mol^{-1}): 28 006, M_w (g mol^{-1}) 32 854 (GPC); Đ: 1.17 (GPC); ^{1}H NMR (500 MHz, CDCl$_3$) δ 3.58 (polymer CH_3O), 2.00–1.66 (polymer CH_2), 1.06–0.70 (polymer CH_3) ppm.

PMMA-co-UIM-MMA 1.5% 11. General procedure for PMMA-co-UIM-MMA polymerization was followed adding methyl methacrylate (1.0 mL, 9.99 mmol), 4-cyano-4-((dodecylsulfanylthiocarbonyl)sulfanyl) pentanoic acid **14** (27 mg, 0.067 mmol) and AIBN **15** (1 mg, 0.0067 mmol) to a schlenk tube containing co-monomer **1** (86 mg, 0.30 mmol) and heated for 5 hours. Yield: 566 mg, 52%; M_n (g mol^{-1}) 15 135, M_w (g mol^{-1}) 20 306 (GPC); Đ: 1.34 (GPC); ^{1}H NMR (500 MHz, CDCl$_3$) δ 7.39 (br. s, 2H, co-monomer imidazole–H), 7.10 (br. s, 2H, co-monomer imidazole–H), 4.22–3.94 (m, 4H, co-monomer CH_2CH_2O), 3.86–3.31 (polymer CH_3O), 2.10–1.60 (polymer CH_2), 1.10–0.58 (polymer CH_3) ppm.

PMMA-co-UIM-MMA 2% 12. General procedure for PMMA-co-UIM-MMA polymerization was followed adding methyl

methacrylate (1.6 mL, 15.0 mmol), 4-cyano-4-((dodecylsulfa-nylthiocarbonyl)sulfanyl) pentanoic acid **14** (12 mg, 0.03 mmol), AIBN **15** (1 mg, 0.006 mmol) and co-monomer **1** (130 mg, 0.45 mmol) to a schlenk tube and heated for 18 hours. Yield: 850 mg, 51%; M_n (g mol^{-1}) 9460, M_w (g mol^{-1}) 16 577 (GPC); Đ: 1.71 (GPC); ^{1}H NMR (500 MHz, CDCl$_3$) δ 7.40 (2H, br s, co-monomer imidazole–H), 7.16 (2H, br s, co-monomer imidazole–H), 4.24–4.00 (4H, m, co-monomer CH_2CH_2O), 3.59 (polymer CH_3O), 2.20–1.55 (polymer CH_2), 1.10–0.50 (polymer CH_3) ppm.

PMMA-co-UIM-MMA 4% 13. General Procedure for PMMA-co-UIM-MMA polymerization was followed adding methyl methacrylate (1.0 mL, 9.99 mmol), 4-cyano-4-((dodecylsulfa-nylthiocarbonyl)sulfanyl) pentanoic acid **14** (27 mg, 0.067 mmol) and AIBN **15** (1 mg, 0.0067 mmol) to a schlenk tube containing co-monomer **1** (345 mg, 1.20 mmol) and heated for 5 hours. Yield: 764 g, 56% M_n (g mol^{-1}) 19 114, M_w (g mol^{-1}) 25 166 (GPC); Đ: 1.32 (GPC); ^{1}H NMR (500 MHz, DMSO-d_6) δ 7.36 (br s, 2H, co-monomer imidazole–H), 7.05 (br s, 2H, co-monomer imidazole–H), 4.11–3.89 (m, 4H, co-monomer CH_2CH_2O), 3.77–3.36 (polymer CH_3O), 2.05–1.60 (polymer CH_2), 1.10–0.58 (polymer CH_3) ppm.

General procedure polystyrene-co-AIC-styrene polymerization. The required amount of styrene co-monomer **2** (if required) and solvent (if required) was transferred to an ampoule with stirrer bar under nitrogen atmosphere. A solution of the required amount of cyanomethyl-dodecyltrithiocarbonate (CTA) **22** (if required) and azobutyroni-trile (AIBN) **15** (if required) dissolved in styrene monomer **16** was also prepared, and the required aliquot of stock solution was added to the ampoule by syringe addition. The reaction mixture was thoroughly degassed by purging with nitrogen for 30 minutes, followed by three freeze–pump–thaw cycles. The reaction mixture was placed into a preheated oil bath at 110 °C and stirred for the specified time. After this time, the flask was immediately cooled to 0 °C to prevent any further polymerization. Precipitation with methanol twice, followed by removal of residual solvent under reduced pressure provided the title material as a flocculent colorless powder.

Polystyrene 17. General procedure for polystyrene-co-AIC-styrene polymerization was followed, styrene **16** (3.64 mL, 31.5 mmol), cyanomethyldodecyltrithiocarbonate **22** (10 mg, 0.03 mmol) and AIBN **15** (1 mg, 0.006 mmol) to a schlenk tube and heated for 18 hours. Yield: 1.45 g, 42%; M_n (g mol^{-1}): 25 562, M_w (g mol^{-1}) 33 969 (GPC); Đ: 1.33 (GPC); ^{1}H NMR (500 MHz, CDCl$_3$) δ 7.32–6.84 (polymer Ar–H), 6.84–6.24 (polymer Ar–H), 2.00–1.65 (polymer CH–Ar), 1.65–1.18 (polymer CH_2CH–Ar) ppm.

Polystyrene-co-AIC-styrene 1.5% 18. General procedure for polystyrene-co-AIC-styrene polymerization was followed adding styrene **16** (0.5 mL, 4.40 mmol), cyanomethyl-dodecyltrithiocarbonate **22** (1.6 mg, 0.005 mmol) and styrene-AIC co-monomer **2** (12.5 mg, 0.035 mmol) and heated for 16 hours. Yield: 255 mg, 54%; M_n (g mol^{-1}): 15 958, M_w (g mol^{-1}) 28 297 (GPC); Đ: 1.77 (GPC); ^{1}H NMR (500 MHz, CDCl$_3$) δ 7.22–6.86 (polymer Ar–H), 6.71–6.26 (polymer Ar–H),

6.02–5.96 (br s, 1H, co-monomer pyridyl–H), 5.10–4.95 (br s, 2H, co-monomer Bn–CH_2), 2.71–2.55 (m, 2H, co-monomer OC(O)CH_2), 2.55–2.34 (m, 2H, co-monomer NHC(O)CH_2), 2.34–2.14 (m, 3H, co-monomer pyridyl–CH_3), 2.14–2.00 (m, 2H, co-monomer CH_2CH_2CH_2), 2.00–1.70 (polymer CH), 1.68–1.16 (polymer CH_2) ppm.

Polystyrene-*co*-AIC-styrene 2.0% 19. General procedure for polystyrene-*co*-AIC-styrene polymerization was followed, styrene **16** (3.64 mL, 31.5 mmol), cyanomethyl-dodecyltrithiocarbonate **22** (10 mg, 0.03 mmol), AIBN **15** (1 mg, 0.006 mmol) and styrene-AIC co-monomer **2** (335 mg, 0.94 mmol) to a schlenk tube and heated for 18 hours. Yield: 945 mg, 26%; M_n (g mol^{-1}): 8053, M_w (g mol^{-1}) 16 173 (GPC); $Đ$: 2.01 (GPC); ^{1}H NMR (500 MHz, CDCl$_3$) δ 7.22–6.86 (polymer Ar–H), 6.71–6.26 (polymer Ar–H), 6.03–5.94 (br s, 1H, co-monomer pyridyl–H), 5.10–4.93 (br s, 2H, co-monomer Bn–CH_2), 2.66–2.53 (m, 2H, co-monomer OC(O)CH_2), 2.51–2.34 (m, 2H, co-monomer NHC(O)CH_2), 2.25–2.12 (m, 3H, co-monomer pyridyl–CH_3), 2.12–1.99 (m, 2H, co-monomer CH_2CH_2CH_2), 1.99–1.68 (polymer CH), 1.68–1.16 (polymer CH_2) ppm.

Polystyrene-*co*-AIC-styrene 5.0% 20. General procedure for polystyrene-*co*-AIC-styrene polymerization was followed, styrene **16** (1.82 mL, 15.7 mmol), cyanomethyl-dodecyltrithiocarbonate **22** (10 mg, 0.03 mmol), AIBN **15** (1 mg, 0.006 mmol) and styrene-AIC co-monomer **2** (335 mg, 0.94 mmol) to a schlenk tube and heated for 18 hours. Yield: 1.01 g, 51%; M_n (g mol^{-1}): 8120, M_w (g mol^{-1}) 16 551 (GPC); $Đ$: 2.04 (GPC); ^{1}H NMR (500 MHz, CDCl$_3$) δ 7.22–6.86 (polymer Ar–H), 6.71–6.26 (polymer Ar–H), 6.03–5.96 (br s, 1H, co-monomer pyridyl–H), 5.10–4.93 (br s, 2H, co-monomer Bn–CH_2), 2.67–2.53 (m, 2H, co-monomer OC(O)CH_2), 2.53–2.39 (m, 2H, co-monomer NHC(O)CH_2), 2.20–2.11 (m, 3H, co-monomer pyridyl–CH_3), 2.11–1.97 (m, 2H, co-monomer CH_2CH_2CH_2), 1.97–1.68 (polymer CH), 1.68–1.16 (polymer CH_2) ppm.

Polystyrene-*co*-AIC-styrene 5.5% 21. General procedure for polystyrene-*co*-AIC-styrene polymerization was followed, styrene **16** (0.5 mL, 4.40 mmol), cyanomethyl-dodecyltrithiocarbonate **22** (1.6 mg, 0.005 mmol) and styrene-AIC co-monomer **2** (93.8 mg, 0.264 mmol) and heated for 16 hours. Yield: 360 mg, 65%; M_n (g mol^{-1}): 11 400, M_w (g mol^{-1}) 20 843 (GPC); $Đ$: 1.82 (GPC); ^{1}H NMR (500 MHz, CDCl$_3$) δ 7.22–6.86 (polymer Ar–H), 6.80–6.25 (polymer Ar–H), 6.05–5.90 (br s, 1H, co-monomer pyridyl–H), 5.13–4.91 (br s, 2H, co-monomer Bn–CH_2), 2.73–2.53 (m, 2H, co-monomer OC(O)CH_2), 2.52–2.32 (m, 2H, co-monomer NHC(O)CH_2), 2.26–2.11 (m, 3H, co-monomer pyridyl–CH_3), 2.11–2.00 (m, 2H, CH_2CH_2CH_2), 2.00–1.68 (polymer CH), 1.68–1.16 (polymer CH_2) ppm.

Differential scanning calorimetry. DSC measurements were performed using a TA Instruments Q2000 heat flux instrument equipped with a liquid nitrogen cooling system. Polymer samples, were prepared by solvent casting 1 : 1 mixtures of co-polymers in dichloromethane solution (20 mg mL^{-1}) of each component by mass. The samples were dried at room tempera-ture for 24 hours, and subsequently annealed in a vacuum oven at 120 °C for 24 hours in order to completely remove any dichloromethane prior to measurements. After drying, the samples with typical weight of ∼5–15 mg were placed in alu-minium pans (hermetic Tzero pans from TA instruments) that were hermetically sealed. Experiments were performed between 20 °C and 180 °C under a helium atmosphere, using heating/cooling scanning rates of 10 °C min^{-1}.

Atomic force microscopy. The samples were prepared by spin coating at 600 rpm, a solution of the 1 : 1 mixture (20 mg of each component in 2 mL of dichloromethane) onto a silicon wafer. Topographical and nanomechanical surface imaging of the polymer blends was carried out under ambient laboratory conditions using Peak Force Quantitative Nanomechanical Mapping (PF-QNM) mode on a Bruker Icon AFM running Nanoscope v9.4 control software. The TESPA-V2 probes (Bruker), with a nominal spring constant of 37 N m^{-1} were selected to give a strong mechanical signal in samples with modulus around 1 GPa. At the start of each experiment the cantilevers were first calibrated using a sapphire surface to obtain the deflection sensitivity, high speed QNM sensitivities at each tapping frequency, and the sync distance delay times. The spring constant was then calibrated using both the thermal noise method and Sader method, the latter required as a check due to the small amplitude of the thermal noise peak with this stiff lever, thus greater error. Spring constants were measured in the range 40–42 N m^{-1}. The relative cali-bration method was used to achieve quantitative nanomecha-nics by calibrating against a known standard, a phase separ-ated blend of PS/LDPE. The tip radius parameter was adjusted to achieve a PS modulus of 3.0 GPa, giving a modulus for the LDPE phase as 60–70 MPa. Images were acquired at a PF tapping frequency of 1 kHz, at 640 or 768 pixel resolution. Peak force was adjusted to achieve a sample deformation of 2 nm. Over time the calibration tends to drift due to changes to the probe hence the contact radius, so the calibration stan-dard was frequently re-imaged, which was used to both recali-brate for subsequent imaging, and also to correct the measure-ments just prior to re-calibration. Film depths were measured by gently scoring the surface with a new razor blade, producing a clean square bottomed scratch about 10 μm in width, which was then imaged using AFM. AFM images were processed and analysed using Nanoscope Analysis v1.9 (Bruker).

Conflicts of interest

There are no conflicts to declare.

Acknowledgements

Dr Martin Walko for assistance in acquiring NMR and IR spectra.

Notes and references

1 D. R. Paul and J. W. Barlow, *J. Macromol. Sci., C, Polym. Rev.*, 1980, **18**, 109–168.
2 J. Runt and J. Huang, in *Handbook of Thermal Analysis and Calorimetry*, ed. S. Cheng, Elsevier Science B.V., 2002, vol. 3, pp. 273–294.
3 M. T. Demeuse, in *High Temperature Polymer Blends*, ed. M. T. DeMeuse, Woodhead Publishing, 2014, pp. 1–13, DOI: 10.1533/9780857099013.1.
4 L. A. Goettler and J. J. Scobbo, in *Polymer Blends Handbook*, ed. L. A. Utracki and C. A. Wilkie, Springer Netherlands, Dordrecht, 2014, pp. 1433–1458, DOI: 10.1007/978-94-007-6064-6_17.
5 L. A. Utracki and M. M. Dumoulin, in *Polypropylene Structure, blends and composites: Volume 2 Copolymers and Blends*, ed. J. Karger-Kocsis, Springer Netherlands, Dordrecht, 1995, pp. 50–94, DOI: 10.1007/978-94-011-0521-7_3.
6 L. M. Robeson, *Polym. Eng. Sci.*, 1984, **24**, 587–597.
7 I. M. Arcana, B. Bundjali, I. Yudistira, B. Jariah and L. Sukria, *Polym. J.*, 2007, **39**, 1337–1344.
8 A. Soroudi and I. Jakubowicz, *Eur. Polym. J.*, 2013, **49**, 2839–2858.
9 K. Hamad, M. Kaseem, Y. G. Ko and F. Deri, *Polym. Sci., Ser. A*, 2014, **56**, 812–829.
10 F. Wu, M. Misra and A. K. Mohanty, *RSC Adv.*, 2019, **9**, 2836–2847.
11 J. L. Koenig, in *Spectroscopy of Polymers*, ed. J. L. Koenig, Elsevier Science, New York, 2nd edn, 1999, pp. 77–145, DOI: 10.1016/B978-044410031-3/50003-7.
12 W. J. MacKnight and F. E. Karasz, in *Comprehensive Polymer Science and Supplements*, ed. G. Allen and J. C. Bevington, Pergamon, Amsterdam, 1989, pp. 111–130, DOI: 10.1016/B978-0-08-096701-1.00207-X.
13 S.-W. Kuo, *J. Polym. Res.*, 2008, **15**, 459–486.
14 T. F. A. De Greef, M. M. J. Smulders, M. Wolffs, A. P. H. J. Schenning, R. P. Sijbesma and E. W. Meijer, *Chem. Rev.*, 2009, **109**, 5687–5754.
15 J. D. Fox and S. J. Rowan, *Macromolecules*, 2009, **42**, 6823–6835.
16 L. Yang, X. Tan, Z. Wang and X. Zhang, *Chem. Rev.*, 2015, **115**, 7196–7239.
17 L. R. Hart, J. L. Harries, B. W. Greenland, H. M. Colquhoun and W. Hayes, *Polym. Chem.*, 2013, **4**, 4860–4860.
18 C. A. Anderson, A. R. Jones, E. M. Briggs, E. J. Novitsky, D. W. Kuykendall, N. R. Sottos and S. C. Zimmerman, *J. Am. Chem. Soc.*, 2013, **135**, 7288–7295.
19 O. J. G. M. Goor, S. I. S. Hendrikse, P. Y. W. Dankers and E. W. Meijer, *Chem. Soc. Rev.*, 2017, **46**, 6621–6637.
20 P. Y. W. Dankers, T. M. Hermans, T. W. Baughman, Y. Kamikawa, R. E. Kieltyka, M. M. C. Bastings, H. M. Janssen, N. A. J. M. Sommerdijk, A. Larsen, M. J. A. van Luyn, A. W. Bosman, E. R. Popa, G. Fytas and E. W. Meijer, *Adv. Mater.*, 2012, **24**, 2703–2709.
21 W. H. Binder and R. Zirbs, *Adv. Polym. Sci.*, 2007, **207**, 1.
22 S. K. Yang and S. C. Zimmerman, *Isr. J. Chem.*, 2013, **53**, 511–520.
23 S. C. Zimmerman and P. S. Corbin, *Struct. Bonding*, 2000, **96**, 63–94.
24 R. P. Sijbesma and E. W. Meijer, *Chem. Commun.*, 2003, 5–16.
25 A. J. Wilson, *Soft Matter*, 2007, **3**, 409–425.
26 P. K. Baruah and S. Khan, *RSC Adv.*, 2013, **3**, 21202–21217.
27 D. A. Leigh, C. C. Robertson, A. M. Z. Slawin and P. I. T. Thomson, *J. Am. Chem. Soc.*, 2013, **135**, 9939–9943.
28 W. P. J. Appel, M. M. L. Nieuwenhuizen, M. Lutz, B. F. M. de Waal, A. R. A. Palmans and E. W. Meijer, *Chem. Sci.*, 2014, **5**, 3735–3745.
29 S. Rayavarapu, S. Kheria, D. R. Shinde, R. G. Gonnade and G. J. Sanjayan, *Org. Biomol. Chem.*, 2017, **15**, 10087–10094.
30 L. Brunsveld, B. J. B. Folmer, E. W. Meijer and R. P. Sijbesma, *Chem. Rev.*, 2001, **101**, 4071–4098.
31 J. M. Pollino and M. Weck, *Chem. Soc. Rev.*, 2005, **34**, 193–207.
32 R. J. Thibault, P. J. Hotchkiss, M. Gray and V. M. Rotello, *J. Am. Chem. Soc.*, 2003, **125**, 11249–11252.
33 T. Park and S. C. Zimmerman, *J. Am. Chem. Soc.*, 2006, **128**, 11582–11590.
34 R. McHale and R. K. O'Reilly, *Macromolecules*, 2012, **45**, 7665–7675.
35 A. Khan, D. M. Haddleton, M. J. Hannon, D. Kukulj and A. Marsh, *Macromolecules*, 1999, **32**, 6560–6564.
36 M. J. Kunz, G. Hayn, R. Saf and W. H. Binder, *J. Polym. Sci., Part A: Polym. Chem.*, 2004, **42**, 661–674.
37 H. Xu, T. B. Norsten, O. Uzun, E. Jeoung and V. M. Rotello, *Chem. Commun.*, 2005, 5157–5159.
38 M. Weck, *Polym. Int.*, 2007, **56**, 453–456.
39 P. Arumugam, H. Xu, S. Srivastava and V. M. Rotello, *Polym. Int.*, 2007, **56**, 461–466.
40 Y. Ishihara, H. Bazzi, V. Toader, F. Godin and H. Sleiman, *Chem. – Eur. J.*, 2007, **13**, 4560–4570.
41 F. Herbst and W. H. Binder, *Polym. Chem.*, 2013, **4**, 3602–3609.
42 J.-H. Wang, O. Altukhov, C.-C. Cheng, F.-C. Chang and S.-W. Kuo, *Soft Matter*, 2013, **9**, 5196–5206.
43 T. Park, S. C. Zimmerman and S. Nakashima, *J. Am. Chem. Soc.*, 2005, **127**, 6520–6521.
44 A. Gooch, N. S. Murphy, N. H. Thomson and A. J. Wilson, *Macromolecules*, 2013, **46**, 9634–9641.
45 A. Gooch, A. M. McGhee, L. C. Renton, J. P. Plante, C. I. Lindsay and A. J. Wilson, *Supramol. Chem.*, 2009, **21**, 12–17.
46 M. L. Pellizzaro, A. M. McGhee, L. C. Renton, M. G. Nix, J. Fisher, W. B. Turnbull and A. J. Wilson, *Chem. – Eur. J.*, 2011, **17**, 14508–14517.

47 A. Gooch, A. M. McGhee, M. L. Pellizzaro, C. I. Lindsay and A. J. Wilson, *Org. Lett.*, 2011, **13**, 240–243.

48 A. M. McGhee, C. Kilner and A. J. Wilson, *Chem. Commun.*, 2008, 344–346.

49 A. Gooch, C. Nedolisa, K. A. Houton, C. I. Lindsay, A. Saiani and A. J. Wilson, *Macromolecules*, 2012, **45**, 4723–4729.

50 C.-H. Wong and S. C. Zimmerman, *Chem. Commun.*, 2013, **49**, 1679–1695.

51 H. M. Coubrough, S. C. C. van der Lubbe, K. Hetherington, A. Minard, C. Pask, M. J. Howard, C. Fonseca Guerra and A. J. Wilson, *Chem. – Eur. J.*, 2019, **25**, 785–795.

52 M. L. Pellizzaro, K. A. Houton and A. J. Wilson, *Chem. Sci.*, 2013, **4**, 1825–1829.

53 H. Shigemitsu, T. Fujisaku, W. Tanaka, R. Kubota, S. Minami, K. Urayama and I. Hamachi, *Nat. Nanotechnol.*, 2018, **13**, 165–172.

54 J. Ruiz-Olles and D. K. Smith, *Chem. Sci.*, 2018, **9**, 5541–5550.

55 E. R. Draper, E. G. B. Eden, T. O. McDonald and D. J. Adams, *Nat. Chem.*, 2015, **7**, 848–852.

56 S. Perrier, *Macromolecules*, 2017, **50**, 7433–7447.

57 G. Moad, E. Rizzardo and S. H. Thang, *Aust. J. Chem.*, 2012, **65**, 985–1076.

58 J. M. G. Cowie and V. Arrighi, *Polymers, Chemistry and Physics of Modern Materials*, CRC Press, Boca Raton, 2007.

59 K. Tanaka, A. Takahara and T. Kajiyama, *Macromolecules*, 1996, **29**, 3232–3239.

60 T. P. Lodge and T. C. B. McLeish, *Macromolecules*, 2000, **33**, 5278–5284.

61 T. P. Lodge, E. R. Wood and J. C. Haley, *J. Polym. Sci., Part B: Polym. Phys.*, 2006, **44**, 756–763.

62 J. Zhao, M. D. Ediger, Y. Sun and L. Yu, *Macromolecules*, 2009, **42**, 6777–6783.

63 D. Hoffman, *Master's*, Michigan Technological University, 2010.

64 B. J. Briscoe, L. Fiori and E. Pelillo, *J. Phys. D: Appl. Phys.*, 1998, **31**, 2395–2405.

65 M. Lorenzoni, L. Evangelio, C. Nicolet, C. Navarro, A. S. Paulo, G. Rius and F. Pérez-Murano, *J. Micro/Nanolithogr., MEMS, MOEMS*, 2015, **14**(1–6), 6.